Whole-exome sequencing validates a preclinical mouse model for the prevention and treatment of cutaneous squamous cell carcinoma

Knatko, Elena V.; Praslicka, Brandon; Higgins, Maureen; Evans, Alan; Purdie, Karin J.; Harwood, Catherine A.

Published in:
Cancer Prevention Research

DOI:
10.1158/1940-6207.CAPR-16-0218

Publication date:
2017

Whole exome sequencing validates a preclinical mouse model for the prevention and treatment of cutaneous squamous cell carcinoma

Elena V. Knatko[1,**], Brandon Praslicka[2,**], Maureen Higgins[1], Alan Evans[3], Karin J. Purdie[4], Catherine A. Harwood[4], Charlotte M. Proby[1], Aikseng Ooi[2,*], and Albena T. Dinkova-Kostova[1,5,*]

[1]*Division of Cancer Research, School of Medicine, University of Dundee, Scotland, United Kingdom*

[2]*Department of Toxicology and Pharmacology, College of Pharmacy, University of Arizona. Tucson, Arizona, USA*

[3]*Department of Pathology, Ninewells Hospital and Medical School, Dundee, Scotland, United Kingdom*

[4]*Centre for Cutaneous Research, Barts and the London Queen Mary University of London, London, United Kingdom*

[5]*Department Pharmacology and Molecular Sciences and Department of Medicine, Johns Hopkins University School of Medicine, Baltimore, Maryland, USA*

*Co-corresponding authors: Aikseng Ooi, Department of Toxicology and Pharmacology, College of Pharmacy, University of Arizona. Tucson, Arizona, USA. Tel.: (+1)-520-626-4294; Email: ooi@pharmacy.arizona.edu and Albena T. Dinkova-Kostova, Division of Cancer Research, School of Medicine, Jacqui Wood Cancer Centre, James Arrott Drive, Dundee DD1 9SY, Scotland, United Kingdom. Tel: (+44)-1382-383386; Email: a.dinkovakostova@dundee.ac.uk

**The first two authors have contributed equally to this study.

Running Title: Whole exome sequencing of mouse cSCC

Disclosure of Potential Conflicts of Interest: None of the authors have any potential conflict of interest to disclose.

Financial Support: This work was supported by Tenovus Scotland, Cancer Research UK (C20953/A10270 and C20953/A18644), and the British Skin Foundation (Project Number 7015). These grants were awarded to ATD-K.

5454 words; 2 tables; 4 figures; 8 supplementary tables; 1 supplementary figure

Abstract

Cutaneous squamous cell carcinomas (cSCC) are among the most common and highly mutated human malignancies. Solar UV radiation is the major factor in the etiology of cSCC. Whole exome sequencing of 18 microdissected tumor samples (cases) derived from SKH-1 hairless mice that had been chronically exposed to solar-simulated UV (SSUV) radiation showed a median point mutation (single nucleotide polymorphism, SNP) rate of 155 per megabase. The majority (78.6%) of the SNPs are C.G>T.A transitions, a characteristic UVR-induced mutational signature. Direct comparison with human cSCC cases showed high overlap in terms of both frequency and type of SNP mutations. Mutations in *Trp53* were detected in 15 of 18 (83%) cases, with 20 of 21 SNP mutations located in the protein DNA binding domain. Strikingly, multiple non-synonymous SNP mutations in genes encoding Notch family members (*Notch1-4)* were present in 10 of 18 (55%) cases. The histopathological spectrum of the mouse cSCC that develop in this model resembles very closely the spectrum of human cSCC. We conclude that the mouse SSUV cSCC accurately represent the histopathological and mutational spectra of the most prevalent tumor suppressors of human cSCC, validating the use of this preclinical model for the prevention and treatment of human cSCC.

Introduction

Keratinocyte (basal and squamous cell) skin cancers are the most common types of human malignancy. Since the 1960s, the average rise in new cases has been 3-8% per year (1). This trend is projected to continue because of depletion of stratospheric ozone, increased exposure to solar radiation, and longer life expectancy. Indeed, cutaneous squamous cell carcinomas (cSCC) are rapidly increasing in incidence, causing significant morbidity and mortality (2). In the 10-year period from 2001 to 2011, Scotland has seen a greater than 50% increase in the incidence of cSCC, with now around 3,000 new cases diagnosed annually and associated escalating healthcare burden and cost (3). In the US, there were estimated 400,000 new cases of cSCC diagnosed in 2012 alone (4). It has been suggested that cSCC represent an under-recognized health issue, and that deaths from cSCC may be as common as deaths from renal and oropharyngeal carcinomas, and melanoma in some parts of the USA (4). This is particularly relevant to patients with multiple cSCC tumors, who have markedly elevated risks of recurrence and metastasis (5).

cSCC typically arise in areas of "field change" on the head and neck where cumulative ultraviolet radiation (UVR) damage from the sun has induced multiple pre-invasive skin lesions. Indeed, UVR is now well recognized as the major factor in the etiology of skin cancer (6). Being the most ubiquitous carcinogen in our environment, UVR is a complete carcinogen (an initiator and a promoter). The solar UV spectrum has two physiologically relevant wavelength components, the shorter and more highly energetic UVB (280–315 nm), which damages the epidermis of the skin, and the longer and more penetrant UVA (315–400 nm), which reaches the underlying dermis. Exposure to solar UVR causes generation of reactive oxygen species (ROS), damage to DNA, lipids and proteins, including DNA damage repair proteins, inflammation, and immunosuppression (1). Together, these deleterious processes contribute to skin photoageing and photocarcinogenesis.

In addition to being among the most common, cSCCs are among the most highly mutated human malignancies, with reported mutation rates of 33-50 per Mb of coding sequence (7, 8). Such extraordinarily high mutation burden makes the possibility for success of a single-target therapy unlikely and highlights the need for development of prevention strategies. To be able to test candidates and develop strategies for skin cancer prevention (and/or treatment) agents, it is essential to have a

preclinical model that closely recapitulates the development of the human disease. One of the most commonly used skin carcinogenesis models is the mutant Harvey-Ras (*Hras*(Q61L))-driven papilloma formation induced by topical treatment with the carcinogen 7,12-dimethylbenz[a]anthracene (DMBA) as the initiator, followed by chronic applications of 12-*O*-tetradecanoylphorbol-13-acetate (TPA) as the promoter. Recently, two independent groups have conducted comprehensive analyses of the mutational landscape of the mouse tumors that form in this model, confirming the driver mutations in *Ras (Hras, Kras and Rras2)* genes with a characteristic DMBA/TPA signature (i.e. A>T and G>T transversions), which occur in a mutually-exclusive fashion in ~90% of the tumors (9, 10). Although mutations in other genes were also identified, most of them did not have the DMBA signature, suggesting that they occur at the later stages during tumor development (9). Whereas the DMBA/TPA model constitutes an excellent model for *RAS*-driven tumors, as demonstrated by the significantly overlapping genes between the mouse tumors that form in this model and human SCC from cervix (44%), head and neck (35%), esophagus (25%) and lung (18%) (9), activating mutations in *RAS* genes are infrequent (<11%) in human cSCC (8). In contrast to human cSCC, the DMBA/TPA-induced mouse tumors carry an average of 5.2 mutations per Mb of coding sequence (10). Overall, tumors that arise in this model do not represent the extraordinarily high level and broad spectrum of mutations that are characteristic of human cSCC.

A second skin carcinogenesis model uses UVB as the carcinogen. However, this model does not reflect sun exposure accurately as the solar UVR that reaches the surface of the earth consists predominantly (~95%) of UVA, with only a small (albeit more carcinogenic) component of UVB wavelengths. The presence of the UVA component is particularly relevant for modelling the development of cSCC in specific high-risk populations, including patients that are undergoing chronic life-long treatment with thiopurine immunosuppressive and anti-inflammatory drugs, such as solid organ transplants recipients and inflammatory bowel disease patients. This is because the combination of UVA and the thiopurine metabolites that incorporate into DNA of proliferating skin cells is highly mutagenic, causing damage to DNA and DNA damage repair proteins (11-13). Indeed, azathioprine treatment photosensitizes the human skin to UVA radiation (14), and the skin cancer risk in organ transplant recipients is ~100-fold greater compared to the general population (15).

To overcome these limitations and build upon the "high-risk" skin carcinogenesis model in SKH-1 hairless mice (16, 17), we have developed a model in which immunocompetent SKH-1 hairless mice are subjected chronically and intermittently to sub-erythemal doses of solar-simulated UVR twice a week for 15 weeks (18). Irradiation is then discontinued, and tumor development is monitored. Although there are no tumor-bearing mice at the end of the period of irradiation, essentially all animals develop tumors during the subsequent 15-20 weeks, in the absence of further exposure to UVR. By use of this model, we found that genetic or pharmacologic upregulation of transcription factor NF-E2 p45-related factor 2 (Nrf2) protects against tumor development (18, 19). Importantly, protection was observed in both immunocompetent mice as well as in animals receiving chronic immunosuppressive therapy with clinically relevant doses of the thiopurine drug azathioprine (18). Very recently, a similar model (with a slightly different irradiation schedule) was employed by Kim *et al.* (20) who found that Fyn, a member of the Src family of protein tyrosine kinases, acts as a redox sensor in a signal transduction cascade induced by exposure to solar-simulated UVR. Using whole exome sequencing of genomic DNA isolated from microdissected tumor tissue, we now show that the cSCCs that arise in this mouse model accurately represent the mutational spectrum of human cSCC.

Together, these findings imply that the "high-risk" solar-simulated UVR skin carcinogenesis mouse model represents a valid model for human cSCC, and justify its use for preclinical testing during the drug development process of topical and/or systemic agents for the prevention and treatment of human cSCC. Furthermore, such testing could be performed on cancer preventive agents, which have UVR-absorbing effects (e.g. sunscreens) and are applied during the irradiation period, as well as on drug candidates, which act by non-UVR-filtering mechanisms and are applied during the tumor development period after cessation of the UV irradiation schedule.

Materials and Methods

Animals

The animal experiments were performed according to the rules and regulations described in the UK Animals (Scientific Procedures) Act 1986. All experimental animals were age-matched and female. The animal study plan was developed after

ethical approval was granted (Project Licence 60/5986), and was further approved by the Named Veterinary Surgeon and the Director of Biological Services of the University of Dundee. SKH-1 hairless mice (initially obtained form Charles River, Germany) were bred and maintained in the Medical School Resource Unit of the University of Dundee on a 12-h light/ 12-h dark cycle and 35% humidity. Throughout the study, the animals had free access to water and pelleted RM1 diet (SDS Ltd., Witham, Essex, UK).

Cutaneous carcinogenesis

Cutaneous carcinogenesis was initiated when the mice were 8-weeks old by subjecting the animals chronically twice a week (on Tuesdays and Fridays) for 15 weeks to solar-simulated UVR (comprised of 2 J/cm^2 UVA and 90 mJ/cm^2 UVB). UVA340 lamps (Q-Lab, Germany) were used as the irradiation source. Irradiation from these lamps simulates the solar UVR from 365 nm to the solar cut-off of 295 nm, with a peak emission at 340 nm. The radiant dose was quantified with a UVB Daavlin Flex Control Integrating Dosimeter, and was further confirmed by use of an external radiometer (X-96 Irradiance Meter; Daavlin, Bryan, OH) before and after each irradiation session. The mice were placed in clear, bedding-free cages and then exposed to UVR. To prevent excessive heating and discomfort to the animals, the irradiation unit (Daavlin, Bryan, OH) was equipped with an electrical fan. Tumors (defined as lesions >1 mm in diameter) that formed on the dorsal skin were measured and mapped once a week.

Sample preparation for whole exome sequencing

The experiment was terminated and the tumors were collected at 20 weeks after completion of the irradiation schedule (i.e., 35 weeks after the onset of irradiation). The tumor samples were snap-frozen in liquid N_2, and stored at –80°C. Normal non-irradiated ventral skin from the same animals was also obtained at the same time and stored under identical conditions. This normal skin served as a source of matched germline DNA. Laser-capture microdissection was employed to enrich for tumor cell populations and prevent contamination by infiltrating inflammatory cells using Zeiss Palm Microbeam microscope (Zeiss, UK). Depending on tumor size and purity (as estimated by examination of H&E reference slides that were prepared in parallel), ~20-90 sections of 8-μm thickness were cut onto 1.0-mm PEN membrane

slides. After staining with 0.05% acid fuchsin (Acros Organics, NJ, USA) in distilled water and 0.05% toluidine blue O (Acros Organics, NJ, USA) in 70% ethanol, the sections were microdissected. Tumor cells were collected into 180 µl ATL buffer (Qiagen, Crawley, UK). Genomic DNA was extracted from tumor cells and from matched normal skin samples (which were crushed into fine powder under liquid N_2) using the QIAamp DNA micro kit (Qiagen, Crawley, UK). Exome capture and sequencing was performed by Oxford Genome Technology (Begbroke, UK) at a sequencing depth of 100x for the tumor DNA, and 50x for the normal skin DNA.

Data analysis

Raw sequencing reads were aligned to the reference genome (UCSC mm9) using Bowtie2, a fast sensitive read alignment software (21). Single Nucleotide Variants (SNV) that differed between tumor and normal samples were identified using SomaticSniper 1.0.5. with somatic score filter set at 40 (22). Small insertions and deletions (INDELs) were called using Platypus, a haplotype-based variant caller for next generation sequencing (23). Mutation calls were annotated using SNPEff (24). Copy number alterations were estimated from the exome sequencing data using the cn.MOPS (Copy Number estimation by a Mixture Of PoissonS') algorithm (25). Matched normal samples processed in the same batch as the tumor samples were used as controls to identify sample specific copy number alterations. The mapped reads for the exome sequencing have been deposited in the Sequence Read Archive (SRA) database (Project Number: PRJNA352449). Mutational signature and statistical analyses were performed in R statistical environment (26).

Results and Discussion

Mouse cutaneous SCC induced by chronic exposure to solar-simulated UVR share similar histopathology with human cutaneous SCC

The development of cSCC in humans is usually associated with chronic sun exposure in early life (27). We therefore subjected mice, beginning at 8 weeks of age, chronically, twice a week for 15 weeks, to solar-simulated UVR (comprised of 2 J/cm^2 UVA and 90 mJ/cm^2 UVB). At termination of the irradiation schedule, none of the animals had developed tumors. However, during the subsequent 20 weeks tumor incidence reached 100% of animals. Visual inspection and mapping of the lesions that

formed on the irradiated dorsal skin of each mouse revealed multiple tumors of variable sizes (**Figure 1**), with tumor multiplicity being on average of 5 tumors per mouse (18, 19). Interestingly, many animals displayed a "field change", also known as "field cancerization" (28), which is a typical representation of the clinical situation. This observation implies that, similar to humans, SKH-1 hairless mice develop multiple primary cSCC in close proximity arising within histologically dysplastic epithelium following chronic intermittent exposure to solar-simulated UVR.

The histopathological spectrum of the mouse cutaneous squamous cell carcinomas (mcSCC) that develop in this model resembles very closely the spectrum of human cutaneous squamous cell carcinomas (hcSCC) (**Figure 2** and **Table 1**). All lesions show clear evidence of background generally severe epidermal dysplasia, often with follicular extension. The lesions group into three main categories: (i) actinic keratosis with no definite invasion; (ii) actinic keratosis with probable early dermal invasion, and (iii) invasive SCC – all in the moderate- to well-differentiated range and some showing extension into the muscle layer. This spectrum of skin tumors is in stark contrast with the tumors that form in the DMBA/TPA skin carcinogenesis model, which are primarily papillomas.

Somatic point mutations manifest prominent UV signature

We performed exome sequencing of 18 microdissected tumor samples (cases) derived from our SKH-1 hairless mice that had been chronically exposed to solar-simulated UVR as described in **Materials and Methods**. Tumor selection was based on size. The size and histopathological characteristics of each individual tumor are described in detail in **Table 1**. Ventral non-irradiated skin from the same animals served as a source of matching normal control DNA. The sequencing revealed a median point mutation (single nucleotide polymorphism, SNP) rate of 155 mutations per megabase with a high of 279 and a low of 12 (**Figure 3A** and **Supplementary Table 1**). The overwhelming majority of SNPs were identified as C.G>T.A transitions (78.6%, **Figure 3B**), a characteristic UVR-induced mutational signature (29), confirming that UVR is the primary cause of mutations in the mcSCC. It is well established that exposure to UVR causes formation of cyclobutane dimers and pyrimidine-pyrimidone (6-4) photoproducts in DNA that initiate C.G>T.A transitions (30-32). Also consistent with a UVR-induced mutational signature, 81.6% of all C.G>T.A mutations in the mouse tumors occurred following a pyrimidine base

(**Figure 3C**), indicative of the formation of dipyrimidine cytosine-containing oncogenic photoproducts (29). In addition, the sequencing revealed a median short insertion and deletion mutation (INDELS) rate of 23.5 per case, including cases harboring zero INDELS to cases with as many as 370 INDELS (**Supplementary Table 2**).

Our results show a remarkably similar mutational signature of the mcSCC to the mutational signature previously described in hcSCC (8, 33). Pickering and colleagues reported that an average of 75% of the mutational events in human patient cases were C>T transitions, and that 85% of these mutations were found at locations following a pyrimidine base (33). Similarly, South and colleagues observed that ~68% of all SNP mutations were C>T transitions in an independent cohort of hcSCC samples (8). Critically, direct comparison of these previously analyzed human hcSCC cases and our mcSCC tumors showed high overlap in terms of both frequency and type of SNP mutations uncovered (**Figure 3D**).

The trinucleotide context of the mutation sites identified in the mcSCC show strong correlation with those in hcSCC reported by Pickering and co-workers, and by South and co-workers, with C > T mutation predominantly occurring around Y(C > T)N trinucleotide (Y represents pyrimidine and N represents A / T / G, or C) **(Figure 3E; Supplementary Figure 1**). Moreover, similar comparison also revealed high correlation in terms of mutation signature between the mcSCC and a UVR associated melanoma mouse model (**Figure 3F, Supplementary Figure 1**).

Copy-number alteration

Pickering and co-workers reported recurring regions of copy number gain on chromosomes 7, 8q, 9q, 14, and 20. To compare the mcSCC to the reported copy number alteration in hcSCC, we estimated copy number alteration from our exome sequencing data. Recurring (in at least 3 of the 18 tumor samples) regions of copy number gains were detected on chromosome 2, 5, 7, 12, 14, 15, and 18 (**Table 2, Supplementary Table 3**). Interestingly, genes located within these regions significantly overlapped with those located in the regions of gains (chromosomes 14, 7, and 8q) reported in hcSCC (**Table 2**, enrichment p-value < 0.05, hypergeometric test). However, regions of loss (chromosomes 5, 6, 9, 11) detected in the mcSCC did not significantly overlap with those in hcSCC.

Mouse cutaneous SCC share similar gene mutations as human cutaneous SCC

Pathway analysis revealed mutations in genes encoding proteins that participate in multiple signaling pathways and cellular processes, such as the Jak-Stat signaling pathway, the neurotrophin signaling pathway, the adipocytokine signaling pathway, T-cell and B-cell receptor signaling pathway, chemokine signaling pathway, MAPK signaling pathway, Hedgehog signaling pathway, p53 signaling pathway, Notch signaling pathway, cytokine-cytokine receptor interactions, ECM-receptor interactions, endocytosis, phagocytosis, melanogenesis, focal adhesion, and metabolism. A complete list is shown in **Supplementary Table 1**.

Particularly striking was the occurrence of mutations in *Trp53* and genes encoding multiple family members of the Notch signaling pathway. In hairless mice, early studies have linked mutations in *Trp53* to exposures to UVB but not to UVA radiation (34). More recently, mutations in the *TP53* gene as well as the genes that encode the NOTCH family of receptors were identified as driver mutations in hcSCC. Interestingly, whereas it has long been known that most if not all hcSCCs contain mutations in the *TP53* gene, it was recently shown that a significant number of hcSCC tumors also harbor mutations in NOTCH receptor encoding genes (8), with *NOTCH1* or *NOTCH2* loss-of-function mutations being present in ~75% of hcSCCs (35). We therefore conducted a detailed analysis on the mutations in *Trp53* and *Notch* genes that were detected in our mcSCC tumor samples.

A total of 21 independent non-synonymous mutations were found in the *Trp53* gene, representing 15 of the 18 (83%) samples sequenced, while 6 out of the 15 samples contained two or more mutations (**Figure 4A**). The mutations were centered on 19 locations distributed across 5 of the 12 exons of the *Trp53* gene. Additionally, 20 of the 21 SNP mutations are located in the DNA binding domain of the protein, suggesting possible loss-of-function consequences. The presence of all of these mutations in the mcSCC tumors was validated by Sanger sequencing (**Supplementary Table 4**).

Mutations in genes encoding the NOTCH family of receptors in hcSCC are usually inactivating and are typically found in the EGF repeat domain. To determine the frequency and location of mutations in these genes we analyzed all four members of the mouse Notch family of receptors (*Notch1-4*) in the mcSCC tumors. Non-synonymous SNP mutations in genes encoding the four Notch family members were found in 10 of the 18 mcSCC tumors sequenced (~55%, **Figure 4B-E**). As in the

hcSCC tumors, seven of the 16 mutations are located in the region encoding the EGF repeat domain of the mouse genes. A total of 6 mutations representing 5 different mcSCC tumors were found in *Notch1* (**Figure 4B**), 3 mutations representing 3 different mcSCC tumors were found in *Notch2* (**Figure 4C**), 5 mutations representing 4 different mcSCC tumors were found in *Notch3* (**Figure 4D**), and 2 mutations representing 2 different mcSCC tumors were found in *Notch4* (**Figure 4E**). We validated the presence of all of these mutations in the mcSCC tumors by Sanger sequencing (**Supplementary Tables 5-8**).

As noted above, loss-of-function mutation in *NOTCH1* or *NOTCH2* occur in ~75% of hcSCC (35), and are considered to be an early event in the development of hcSCC (8). Such inactivating mutations are consistent with the role of Notch signaling in skin, where in contrast to most other tissues, Notch1 negatively regulates keratinocyte self-renewal, promotes differentiation and acts as a tumor suppressor through a number of cell autonomous as well as non-cell autonomous growth control mechanisms (36-41). The high frequency of mutations in *Notch1-4* in our mcSCC tumors, which often form areas of field cancerization, is in close agreement with a recent report showing that in mice, loss of mesenchymal Notch signaling leads to field cancerization and multifocal epithelial tumors (42). It was suggested that this could be due to the role of Notch in inhibiting activator protein-1 (AP-1)-mediated transcription of secreted growth factors, proteases, and extracellular matrix proteins. The same study showed that Notch signaling is suppressed in stromal fields adjacent to cutaneous premalignant actinic keratosis lesions surgically excised from human patients. In addition, persistent suppression of Notch signaling, accompanied by enhanced activity of AP-1, is induced in the dermis of human skin explants and dermal fibroblast upon exposure to UVA, but not UVB radiation (42), highlighting the importance of the UVA component of the solar UVR in the development of cSCC.

Conclusion

Taken together, data presented in this study show that the skin tumors that develop in this mouse model are similar to human cSCC tumors in terms of histopathology, mutational characteristics, and UVR-induced mutational signature. We conclude that by: (i) using UVR as the carcinogen, (ii) incorporating both the UVA and the UVB components of the solar UVR at their natural ratio, and (iii)

employing chronic but intermittent irradiation schedule, this mouse skin carcinogenesis model has high relevance to the human disease. We propose the use of the model for mechanistic studies aiming to further our understanding of cSCC development, as well as for testing potential prevention and treatment strategies for human cSCC.

Acknowledgments

We thank Oxford Genome Technology for performing the whole exome sequencing, and Andrew Cassidy (University of Dundee) for Sanger sequencing.

References

1. Alam M, Ratner D. Cutaneous squamous-cell carcinoma. N Engl J Med. 2001;344:975-83.
2. Jennings L, Schmults CD. Management of high-risk cutaneous squamous cell carcinoma. J Clin Aesthet Dermatol. 2010;3:39-48.
3. (www.isdscotland.org/Health-Topics/Cancer/Cancer-Statistics/Skin/#squamousDavid)
4. Karia PS, Han J, Schmults CD. Cutaneous squamous cell carcinoma: estimated incidence of disease, nodal metastasis, and deaths from disease in the United States, 2012. J Am Acad Dermatol. 2013;68:957-66.
5. Levine DE, Karia PS, Schmults CD. Outcomes of Patients With Multiple Cutaneous Squamous Cell Carcinomas: A 10-Year Single-Institution Cohort Study. JAMA Dermatology. 2015;151:1220-5.
6. de Gruijl FR. Skin cancer and solar UV radiation. Eur J Cancer. 1999;35:2003-9.
7. Durinck S, Ho C, Wang NJ, Liao W, Jakkula LR, Collisson EA, et al. Temporal dissection of tumorigenesis in primary cancers. Cancer Discovery. 2011;1:137-43.
8. South AP, Purdie KJ, Watt SA, Haldenby S, den Breems NY, Dimon M, et al. NOTCH1 mutations occur early during cutaneous squamous cell carcinogenesis. J Invest Dermatol. 2014;134:2630-8.
9. Nassar D, Latil M, Boeckx B, Lambrechts D, Blanpain C. Genomic landscape of carcinogen-induced and genetically induced mouse skin squamous cell carcinoma. Nat Med. 2015;21:946-54.
10. McCreery MQ, Halliwill KD, Chin D, Delrosario R, Hirst G, Vuong P, et al. Evolution of metastasis revealed by mutational landscapes of chemically induced skin cancers. Nat Med. 2015;21:1514-20.
11. O'Donovan P, Perrett CM, Zhang X, Montaner B, Xu YZ, Harwood CA, et al. Azathioprine and UVA light generate mutagenic oxidative DNA damage. Science. 2005;309:1871-4.
12. Brem R, Karran P. Oxidation-mediated DNA cross-linking contributes to the toxicity of 6-thioguanine in human cells. Cancer Res. 2012;72:4787-95.
13. Karran P, Attard N. Thiopurines in current medical practice: molecular mechanisms and contributions to therapy-related cancer. Nat Rev Cancer. 2008;8:24-36.
14. Perrett CM, Walker SL, O'Donovan P, Warwick J, Harwood CA, Karran P, et al. Azathioprine treatment photosensitizes human skin to ultraviolet A radiation. Br J Dermatol. 2008;159:198-204.
15. Harwood CA, Mesher D, McGregor JM, Mitchell L, Leedham-Green M, Raftery M, et al. A surveillance model for skin cancer in organ transplant recipients: a 22-year prospective study in an ethnically diverse population. Am J Transplant. 2013;13:119-29.
16. Lu YP, Lou YR, Xie JG, Peng QY, Liao J, Yang CS, et al. Topical applications of caffeine or (-)-epigallocatechin gallate (EGCG) inhibit carcinogenesis and selectively increase apoptosis in UVB-induced skin tumors in mice. Proc Natl Acad Sci U S A. 2002;99:12455-60.
17. Michna L, Wagner GC, Lou YR, Xie JG, Peng QY, Lin Y, et al. Inhibitory effects of voluntary running wheel exercise on UVB-induced skin carcinogenesis in SKH-1 mice. Carcinogenesis. 2006;27:2108-15.

18. Knatko EV, Ibbotson SH, Zhang Y, Higgins M, Fahey JW, Talalay P, et al. Nrf2 Activation Protects against Solar-Simulated Ultraviolet Radiation in Mice and Humans. Cancer Prev Res (Phila). 2015;8:475-86.
19. Knatko EV, Higgins M, Fahey JW, Dinkova-Kostova AT. Loss of Nrf2 abrogates the protective effect of Keap1 downregulation in a preclinical model of cutaneous squamous cell carcinoma. Scientific reports. 2016;6:25804.
20. Kim JE, Roh E, Lee MH, Yu DH, Kim DJ, Lim TG, et al. Fyn is a redox sensor involved in solar ultraviolet light-induced signal transduction in skin carcinogenesis. Oncogene. 2016;35:4091-101.
21. Langmead B, Trapnell C, Pop M, Salzberg SL. Ultrafast and memory-efficient alignment of short DNA sequences to the human genome. Genome Biol. 2009;10:R25.
22. Larson DE, Harris CC, Chen K, Koboldt DC, Abbott TE, Dooling DJ, et al. SomaticSniper: identification of somatic point mutations in whole genome sequencing data. Bioinformatics. 2012;28:311-7.
23. Rimmer A, Phan H, Mathieson I, Iqbal Z, Twigg SR, Consortium WGS, et al. Integrating mapping-, assembly- and haplotype-based approaches for calling variants in clinical sequencing applications. Nat Genet. 2014;46:912-8.
24. Cingolani P, Platts A, Wang le L, Coon M, Nguyen T, Wang L, et al. A program for annotating and predicting the effects of single nucleotide polymorphisms, SnpEff: SNPs in the genome of Drosophila melanogaster strain w1118; iso-2; iso-3. Fly. 2012;6:80-92.
25. Klambauer G1, Schwarzbauer K, Mayr A, Clevert DA, Mitterecker A, Bodenhofer U, Hochreiter S. cn.MOPS: mixture of Poissons for discovering copy number variations in next-generation sequencing data with a low false discovery rate. Nucleic Acids Res. 2012;40:e69.
26. Team RC. R: A language and environment for statistical computing. 2013.
27. Leiter U, Eigentler T, Garbe C. Epidemiology of skin cancer. Adv Exp Med Biol. 2014;810:120-40.
28. Slaughter DP, Southwick HW, Smejkal W. Field cancerization in oral stratified squamous epithelium; clinical implications of multicentric origin. Cancer. 1953;6:963-8.
29. Brash DE, Rudolph JA, Simon JA, Lin A, McKenna GJ, Baden HP, et al. A role for sunlight in skin cancer: UV-induced p53 mutations in squamous cell carcinoma. Proc Natl Acad Sci U S A. 1991;88:10124-8.
30. Sutherland BM, Carrier WL, Setlow RB. Pyrimidine dimers in the DNA of Paramecium aurelia. Biophys J. 1968;8:490-9.
31. Varghese AJ, Patrick MH. Cytosine derived heteroadduct formation in ultraviolet-irradiated DNA. Nature. 1969;223:299-300.
32. Glickman BW, Schaaper RM, Haseltine WA, Dunn RL, Brash DE. The C-C (6-4) UV photoproduct is mutagenic in Escherichia coli. Proc Natl Acad Sci U S A. 1986;83:6945-9.
33. Pickering CR, Zhou JH, Lee JJ, Drummond JA, Peng SA, Saade RE, et al. Mutational landscape of aggressive cutaneous squamous cell carcinoma. Clin Cancer Res. 2014;20:6582-92.
34. van Kranen HJ, de Gruijl FR. Mutations in cancer genes of UV-induced skin tumors of hairless mice. J Epidemiol. 1999;9:S58-65.
35. Wang NJ, Sanborn Z, Arnett KL, Bayston LJ, Liao W, Proby CM, et al. Loss-of-function mutations in Notch receptors in cutaneous and lung squamous cell carcinoma. Proc Natl Acad Sci U S A. 2011;108:17761-6.

36. Nicolas M, Wolfer A, Raj K, Kummer JA, Mill P, van Noort M, et al. Notch1 functions as a tumor suppressor in mouse skin. Nat Genet. 2003;33:416-21.
37. Dotto GP. Notch tumor suppressor function. Oncogene. 2008;27:5115-23.
38. Watt FM, Estrach S, Ambler CA. Epidermal Notch signalling: differentiation, cancer and adhesion. Curr Opin Cell Biol. 2008;20:171-9.
39. Demehri S, Turkoz A, Kopan R. Epidermal Notch1 loss promotes skin tumorigenesis by impacting the stromal microenvironment. Cancer Cell. 2009;16:55-66.
40. Restivo G, Nguyen BC, Dziunycz P, Ristorcelli E, Ryan RJ, Ozuysal OY, et al. IRF6 is a mediator of Notch pro-differentiation and tumour suppressive function in keratinocytes. EMBO J. 2011;30:4571-85.
41. Williams SE, Beronja S, Pasolli HA, Fuchs E. Asymmetric cell divisions promote Notch-dependent epidermal differentiation. Nature. 2011;470:353-8.
42. Hu B, Castillo E, Harewood L, Ostano P, Reymond A, Dummer R, et al. Multifocal epithelial tumors and field cancerization from loss of mesenchymal CSL signaling. Cell. 2012;149:1207-20.

Figure Legends

Figure 1. Macroscopic appearance of lesions that form in SKH-1 hairless mice following chronic exposure to solar-simulated UVR. Female SKH-1 hairless mice were exposed chronically twice a week for 15 weeks to solar-simulated UVR (comprised of 2 J/cm^2 UVA and 90 mJ/cm^2 UVB) beginning at 8 weeks of age. The experiment was terminated 20 weeks after the end of the irradiation schedule. Examples of typical "field cancerization" of the skin of three animals at termination of the experiment (study week 35).

Figure 2. Histopathological spectrum of lesions that form in SKH-1 hairless mice following chronic exposure to solar-simulated UVR. (A) Low grade (basal layer) epidermal dysplasia in perilesional skin; **(B)** Typical actinic keratosis with epidermal thickening associated with hyper and parakeratosis; **(C)** "Bowenoid" actinic keratosis amounting to carcinoma in situ; **(D)** higher power (400x) image of the same tumor (C) showing severe cytological atypia with loss of cell polarity, single cell dyskeratosis (arrow) and mitosis (arrow); **(E)** invasive SCC; note warty Bowenoid actinic keratosis overlying deeply invasive moderately differentiated carcinoma; **(F)** higher power (200x) image of the same tumor (E) showing islands of invasive carcinoma with stromal desmoplasia (arrow); **(G)** early invasion by SCC; **(H)** higher power (200x) image of the same tumor (I); note the irregular budding with a tongue of squamous cells extending into stroma (arrow), as well as single cell invasion (arrow); **(I)** invasive SCC abutting a band of skeletal muscle tissue; **(J)** higher power (200x) image of the same tumor (G) showing deep invasion by SCC cells encroaching onto skeletal muscle (arrows).

Figure 3. Mutational signature of solar-simulated UVR-induced mcSCC tumors. **(A)** Total number of unique SNPs detected per tumor; the blue line indicates average across all tumors. **(B)** Pie chart of SNP frequencies indicating C>T (beige), C>G (purple), C>A (teal), C > T (green) A>T (green), A>G (blue), and A>C (white). **(C)** Frequency of base preceding each unique SNP mutation. **(D)** Mutation frequency of both transitions and transversions from hcSCC sequencing data from Pickering et al. (red circles) and South et al. (green circles), and in solar-simulated UVR-induced mcSCC tumors from this study (blue triangles). **(E)** Comparison of trinucleotide

context of SNP mutations found in hcSCC reported by Pickering et al. (red dots), hcSCC reported by South et al. (green dots), and our mcSCC samples (blue triangles). **(F)** Comparison of trinucleotide context of SNP mutations found in a mouse UV-induced melanoma model (m-UV, red squares) and our mcSCC samples (blue triangles).

Figure 4. Schematic representation of *Trp53* and *Notch* family nonsynonymous mutations in solar-simulated UVR-induced mcSCC tumors. For all genes, exons are separated by blue lines starting with exon 1 on the left hand side. Mutations are indicated by red lines within the corresponding exons. Tumor case number, cDNA base pair change, and corresponding amino acid change are indicated above each mutation. Asterisks indicate a change to a stop codon. Numbers below each mutation indicate chromosome location. Location of unique non synonymous mutations in *Trp53* **(A)**, *Notch*1 **(B)**, *Notch*2 **(C)**, *Notch*3 **(D)**, and *Notch*4 **(E)**.

Table 1. Histopathological characteristics of cutaneous tumors that form in SKH-1 hairless mice following chronic exposure to solar-simulated UVR.

Case (#)	Size (mm^3)	Histopathological characteristics
379	33.5	Invasive moderately differentiated SCC arising from severely dysplastic epidermis; Invasive into muscle
442	28	Severely dysplastic actinic keratosis extending into multiple hair follicles
252	472	Invasive moderately differentiated SCC with focal ulceration
446	56.7	Invasive moderately differentiated SCC arising from severely dysplastic epidermis; Deeply invasive into muscle
164	18.2	Severely dysplastic actinic keratosis
873	13.7	Severely dysplastic actinic keratosis
334	37.9	Invasive well differentiated SCC arising from severely dysplastic epidermis; the invasive tumour has a broad invasive front.
444	4.6	Severely dysplastic actinic keratosis
441	21.18	Severely dysplastic actinic keratosis with extension into hair follicles and focal early dermal invasion by SCC
1310	8.2	Invasive well differentiated SCC arising from severely dysplastic epidermis
168	9.6	Severely dysplastic actinic keratosis with focal early dermal invasion by SCC
278	11.9	Invasive moderately differentiated SCC arising from severely dysplastic epidermis
124	53.2	Invasive moderately differentiated SCC; Invasive close to muscle
131	25.8	Severely dysplastic actinic keratosis extending into multiple hair follicles
876	3.6	Severely dysplastic actinic keratosis with focal early dermal invasion by SCC
134	35.5	Invasive well differentiated SCC arising from severely dysplastic actinic keratosis
874	20.6	Invasive moderately to well differentiated SCC arising from severely dysplastic epidermis
272	904	Invasive well differentiated squamous cell carcinoma arising from severely dysplastic epidermis

Table 2. Copy number gain regions found in mcSCC and the corresponding regions and overlapping genes reported in hcSCC

Gain Regions in mcSCC	Gain Regions reported in hcSCC	Overlapping genes (Official gene symbols, human)
chr14:3592398-98303604	chr14	GCH1, PNP, TGM1, PTGDR, PTGER2, DAD1, APEX1, CEBPE, BCL2L2, NFATC4, PCK2, PABPN1, REC8, CDKN3, PARP2, RNASE6, CNIH1, EFS, IRF9, PRMT5, NEDD8, NRL, PSME1, TM9SF1, CGRRF1, FERMT2, TEP1, SUPT16H, IPO4, MDP1, OSGEP, BMP4, CIDEB, AJUBA, RNASE1, SLC7A8, TINF2, LRP10, DLGAP5, TOX4, SALL2, C14orf166, ZNF219, HAUS4, C14orf119, AP5M1, TMEM55B, METTL3, LTB4R2, RNASE4, OR11H4, RPGRIP1, SLC22A17, OTX2, C14orf93, REM2, METTL17, DCAF11, C14orf37, MRPL52, FBXO34, JPH4, PSMB11, TTC5, IL25, SOCS4, CMTM5, RNASE11, OR4K5, OR4K2, OR4N5, THTPA, NAA30, TXNDC16, CCNB1IP1, RNASE9, RNASE10, SAMD4A, NYNRIN, ARHGEF40, OR6S1, MMP14, LTB4R, NDRG2, ACIN1, GMPR2, ADCY4, KHNYN, RAB2B, OR11H6, OR10G3, GPR137C, OXA1L, RIPK3, RABGGTA, RNF31, PPP1R3E, DDHD1, LGALS3, GMFB, EXOC5, NID2, GNG2, SLC39A2, EMC9, GNPNAT1, STYX, OR4E2, PELI2, NOP9, FITM1, DHRS1, NGDN, MAPK1IP1L, ATG14, OR5AU1, SLC35F4, AP1G2, ERO1L, TMEM260, DHRS4, OR4M1, KLHL33, ZFHX2, CMA1, PSMB5, WDHD1, CBLN3, ABHD4, CDH24, TSSK4, MYH7, OR4L1, CHD8, OR4K1, ANG, HNRNPC, LRRC16B, EDDM3B, RNASE13, CPNE6, TMEM253, OR4K15, RNASE12, PSME2, OR10G2, SLC7A7, CTSG, RNASE2, MYH6, OR11G2, OR4N2, GZMH
	chr8q	POLR3D
chr14:3122492-25912484	chr14	C14orf166, NID2, GNG2
chr14:30432550-47466147	chr14	PTGDR, PTGER2, CDKN3, CNIH1, FERMT2, BMP4, TXNDC16, GPR137C, DDHD1, GMFB, GNPNAT1, STYX, ERO1L
chr14:49992651-78114658	chr14	PNP, TGM1, DAD1, APEX1, CEBPE, BCL2L2, NFATC4, PCK2, PABPN1, REC8, PARP2, RNASE6, EFS, IRF9, PRMT5, NEDD8, NRL, PSME1, TM9SF1, TEP1, SUPT16H, IPO4, MDP1, OSGEP, CIDEB, AJUBA, RNASE1, SLC7A8, TINF2, LRP10, TOX4, SALL2, ZNF219, HAUS4, C14orf119, TMEM55B, METTL3, LTB4R2, RNASE4, OR11H4, RPGRIP1, SLC22A17, C14orf93, REM2, METTL17, DCAF11, C14orf37, MRPL52, JPH4, PSMB11, TTC5, IL25, CMTM5, RNASE11, OR4K5, OR4K2, OR4N5, THTPA, CCNB1IP1, RNASE9, RNASE10, NYNRIN, ARHGEF40, OR6S1, MMP14, LTB4R, NDRG2, ACIN1, GMPR2, ADCY4, KHNYN, RAB2B, OR11H6, OR10G3, OXA1L, RIPK3, RABGGTA, RNF31, PPP1R3E, SLC39A2, EMC9, OR4E2, NOP9, FITM1, DHRS1, NGDN, OR5AU1, AP1G2, DHRS4, OR4M1, KLHL33, ZFHX2, CMA1, PSMB5, CBLN3, ABHD4, CDH24, TSSK4, MYH7, OR4L1, CHD8, OR4K1, ANG, HNRNPC, LRRC16B, EDDM3B, RNASE13, CPNE6, TMEM253, OR4K15, RNASE12, PSME2, OR10G2, SLC7A7, CTSG, RNASE2, MYH6, OR11G2, OR4N2, GZMH
	chr8q	POLR3D
chr15:51929767-56964852	chr8q	NOV, TNFRSF11B, HAS2, ENPP2, DSCC1, SNTB1, MTBP, MED30, SLC30A8, MAL2, COL14A1, EXT1, TAF2, COLEC10, DEPTOR, SAMD12, MRPL13
chr15:76520787-76813255	chr8q	RECQL4, C8orf33, MFSD3, C8orf82, ZNF7, ZNF250, ARHGAP39, RPL8, LRRC14, LRRC24, ZNF251, GPT
chr15:55432364-55895042	chr8q	SNTB1
chr15:31348828-40614922	chr8q	RPL30, SDC2, FZD6, KLF10, HRSP12, SLC25A32, DCAF13, ODF1, SPAG1, LRP12, RNF19A, UBR5, CPQ, LAPTM4B, BAALC, MTDH, DCSTAMP, TSPYL5, OSR2, CTHRC1, DPYS, MATN2, KCNS2, SNX31, ANKRD46, GRHL2, PABPC1, POP1, NIPAL2, STK3, VPS13B, NCALD, ERICH5, YWHAZ, RRM2B, FBXO43, RGS22, POLR2K, ZNF706
chr15:40828793-128800223	chr8q	PLEC, EIF3E, BAI1, LY6H, NOV, TNFRSF11B, SQLE, TG, TSTA3, LY6D, JRK, EIF3H, WISP1, FOXH1, EBAG9, RECQL4, NDUFB9, GPR20, HAS2, PSCA, ENPP2, KHDRBS3, RNF139, ZHX1, DSCC1, EXOSC4, ATAD2, BOP1, RHPN1, ST3GAL1, ASAP1, DGAT1, KIFC2, LYNX1, FBXL6, TRPS1, EMC2, KIAA0196, ZHX2, ZC3H3, ARC, PHF20L1, FAM49B, SNTB1, SYBU, WDYHV1, ENY2, SLURP1, MTBP, C8orf33, DERL1, SHARPIN, NUDCD1, FBXO32, NSMCE2, GSDMD, MFSD3, MED30, FAM83A, PPP1R16A, FAM91A1, SLC30A8, MAL2, SLC39A4, FAM83H, ZNF623, PKHD1L1, MAPK15, ZFAT, AARD, C8orf82, TBC1D31, TMEM74, RSPO2, ZNF707, FAM84B, COL14A1, OC90, EPPK1, TRHR, ZNF7, ANXA13, KCNQ3, PTP4A3, TONSL, KCNV1, EEF1D, OXR1, ZNF250, ARHGAP39, DENND3, EXT1, MYC, TAF2, COLEC10, RPL8, TRMT12, DEPTOR, CYHR1, ADCK5, LRRC6, ABRA, SAMD12, ADCY8, ANGPT1, GPAA1, RAD21, CPSF1, LRRC14, CHRAC1, GRINA, TOP1MT, COL22A1, EFR3A, SCRIB, MROH1, TMEM65, GML, HGH1, MAF1, TMEM71, PARP10, CYC1, NDRG1, PYCRL, LY6E, KCNK9, SLC52A2, TATDN1, ZFP41, MAFA, CSMD3, VPS28, GSDMC, SLC45A4, HSF1, AGO2, TRAPPC9, NAPRT, SCX, LRRC24, ZNF251, MRPL13, OPLAH, THEM6, CYP11B2, SCRT1, CYP11B1, SPATC1, TIGD5, HHLA1, GPT
chr12:75558256-91008747	chr14	SPTB, LTBP2, ARG2, ESR2, DLST, FNTB, MAX, PGF, TGFB3, NUMB, EIF2S1, ERH, PIGH, ABCD4, FOS, MED6, ALDH6A1, ALKBH1, PNMA1, BATF, NPC2, TMED10, ZBTB25, POMT2, FCF1, ATP6V1D, COQ6, ADCK1, EIF2B2, SLC39A9, PSEN1, VSX2, GSTZ1, AHSA1, PLEK2, AREL1, VASH1, ZBTB1, TTLL5, ZFYVE26, SIPA1L1, DCAF4, MPP5, FUT8, FLVCR2, GPATCH2L, EXD2, SYNJ2BP, GPHN, ZNF410, NGB, ZFYVE1, C14orf169, IRF2BPL, ACYP1, IFT43, JDP2, SLIRP, RPS6KL1, NEK9, CIPC, ISCA2, PLEKHD1, AKAP5, KCNH5, CHURC1, PROX2, GPHB5, DCAF5, TMEM229B, GALNT16, ELMSAN1, TMED8, GPX2, SPTLC2, ZC2HC1C, ACOT2, SLC10A1, ZFP36L1, ANGEL1, TMEM63C, DNAL1, ENTPD5, VTI1B, C14orf1, PTGR2, KIAA0247, PCNX, VRTN, WDR89, ACOT4, ZDHHC22, RAD51B, TTC9, ACTN1, MTHFD1, SNW1, SYNE2, RHOJ, SMOC1, SLC8A3, ADAM21, RGS6, HSPA2, ESRRB, PAPLN, CCDC176, MAP3K9, PLEKHG3, SYNDIG1L, YLPM1, MLH3, RDH11, SGPP1, RDH12, PLEKHH1, CCDC177, DPF3, ACOT1
	chr7	PPP2R5E
chr12:113121116-119215446	chr14	BRF1, JAG2, MTA1, AKT1, SIVA1, CDCA4, TMEM121, NUDT14, TDRD9, PACS2, PLD4, TMEM179, KIF26A, RD3L, ZBTB42, CRIP1, BTBD6, CEP170B, C14orf180, C14orf80, INF2, TEX22, ADSSL1, ASPG, C14orf2
	chr7	PTPRN2, VIPR2, NCAPG2, CDCA7L, WDR60, ESYT2, RAPGEF5

Figure 1

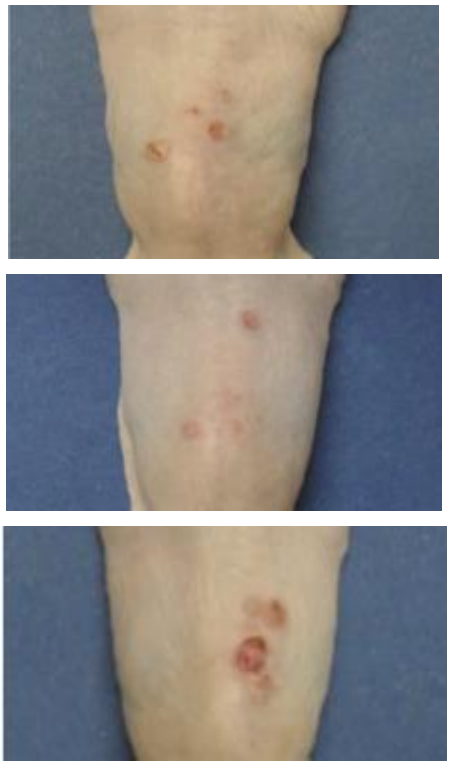

Figure 2

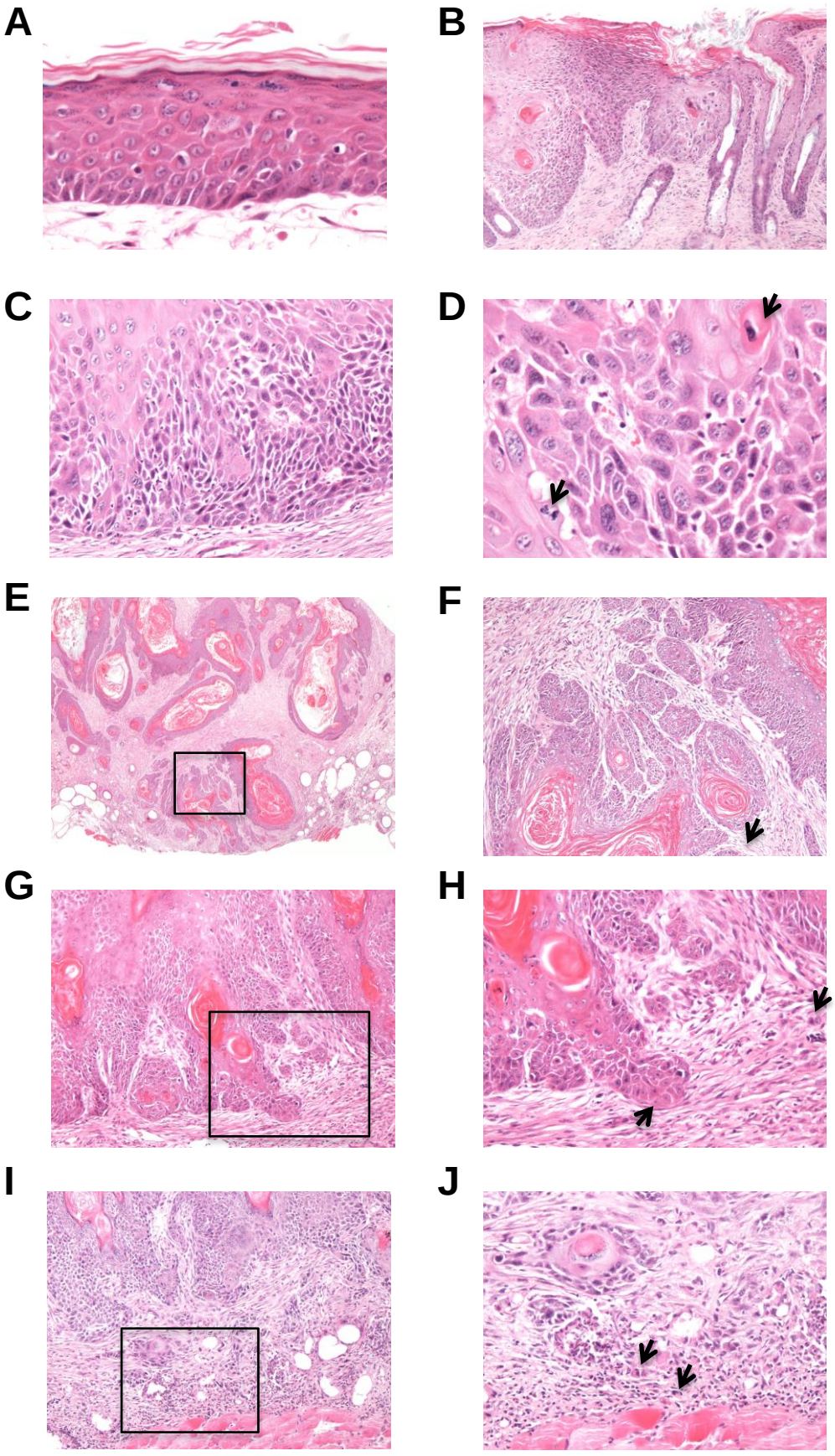

Figure 3

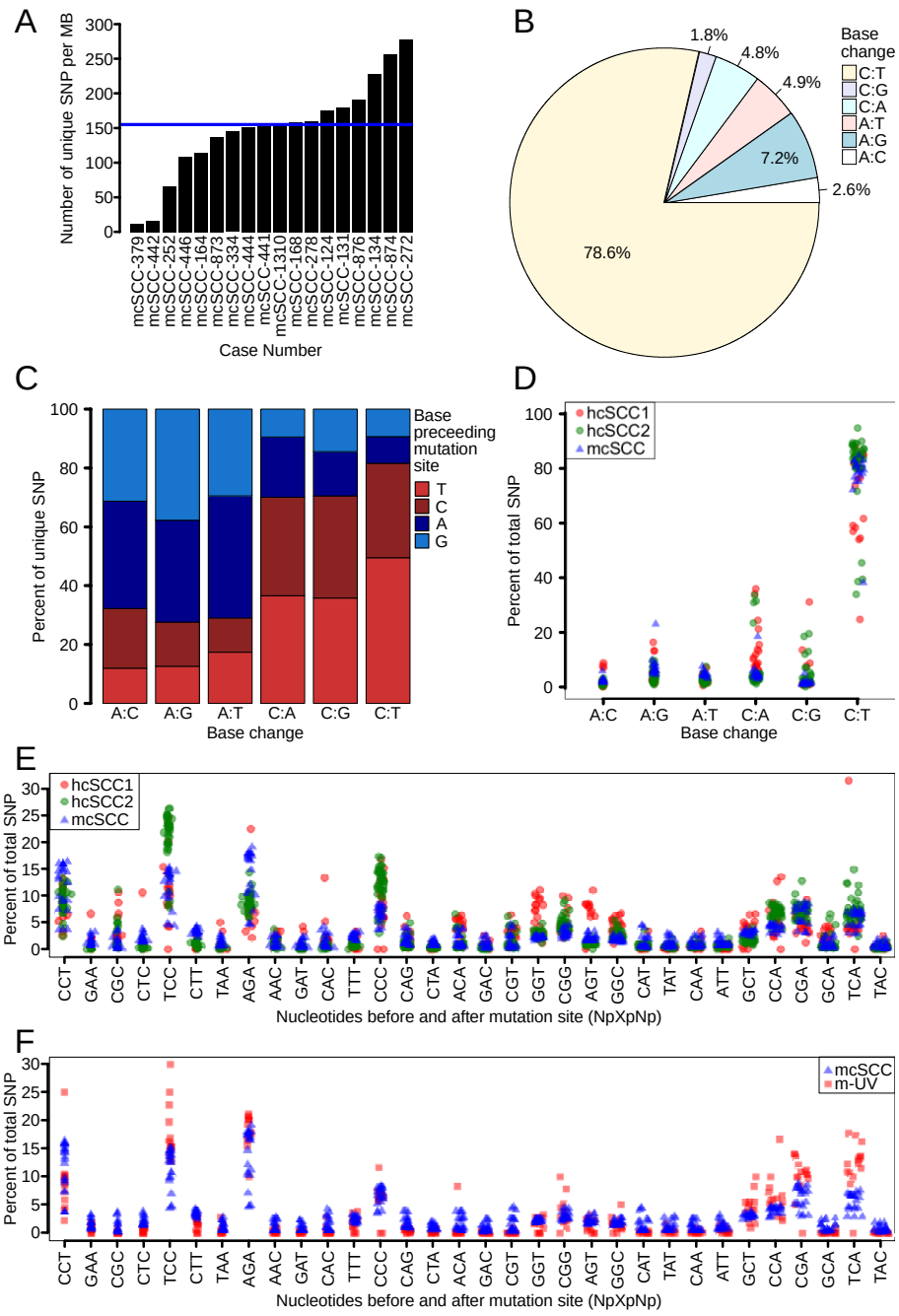
A
Number of unique SNP per MB
300
250
200
150
100
50
0
mcSCC-379
mcSCC-442
mcSCC-252
mcSCC-446
mcSCC-164
mcSCC-873
mcSCC-334
mcSCC-444
mcSCC-441
mcSCC-1310
mcSCC-168
mcSCC-278
mcSCC-124
mcSCC-131
mcSCC-876
mcSCC-134
mcSCC-874
mcSCC-272
Case Number
B
1.8%
4.8%
4.9%
7.2%
2.6%
78.6%
Base change
C:T
C:G
C:A
A:T
A:G
A:C
C
Percent of unique SNP
100
80
60
40
20
0
A:C
A:G
A:T
C:A
C:G
C:T
Base change
Base preceeding mutation site
T
C
A
G
D
Percent of total SNP
hcSCC1
hcSCC2
mcSCC
Base change
E
Percent of total SNP
hcSCC1
hcSCC2
mcSCC
CCT GAA CGC CTC TCC CTT TAA AGA AAC GAT CAC TTT CCC CAG CTA ACA GAC CGT GGT CGG AGT GGC CAT TAT CAA ATT GCT CCA CGA GCA TCA TAC
Nucleotides before and after mutation site (NpXpNp)
F
Percent of total SNP
mcSCC
m-UV
CCT GAA CGC CTC TCC CTT TAA AGA AAC GAT CAC TTT CCC CAG CTA ACA GAC CGT GGT CGG AGT GGC CAT TAT CAA ATT GCT CCA CGA GCA TCA TAC
Nucleotides before and after mutation site (NpXpNp)

Figure 4

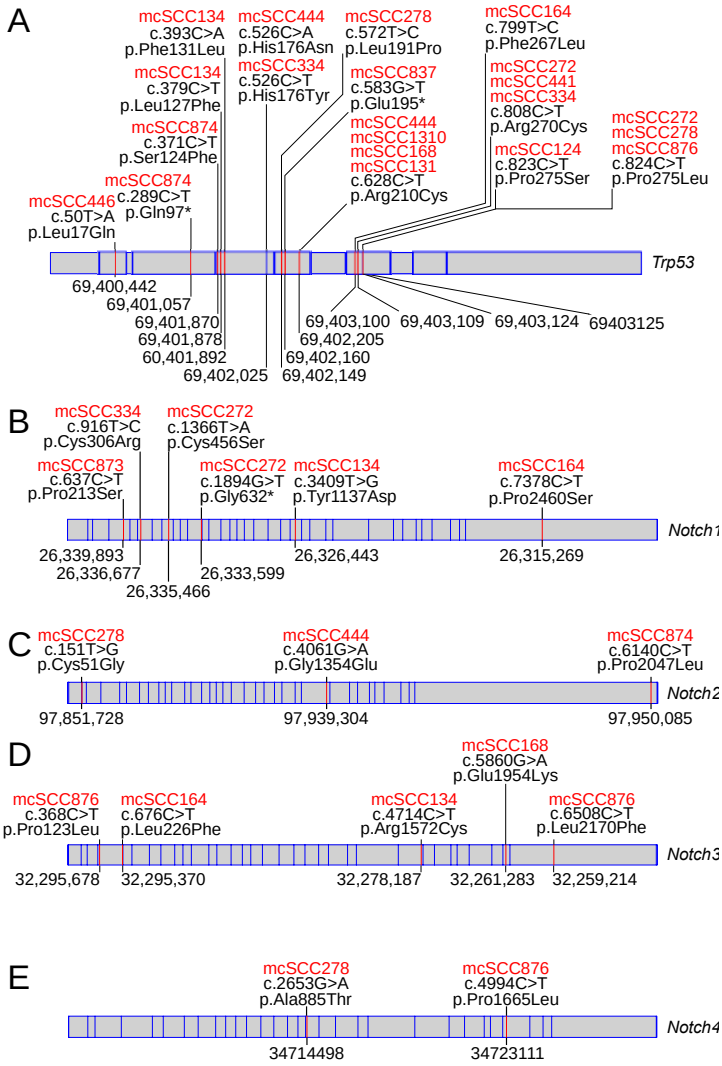
A
mcSCC134
c.393C>A
p.Phe131Leu
mcSCC444
c.526C>A
p.His176Asn
mcSCC278
c.572T>C
p.Leu191Pro
mcSCC164
c.799T>C
p.Phe267Leu
mcSCC134
c.379C>T
p.Leu127Phe
mcSCC334
c.526C>T
p.His176Tyr
mcSCC837
c.583G>T
p.Glu195*
mcSCC272
mcSCC441
mcSCC334
c.808C>T
p.Arg270Cys
mcSCC874
c.371C>T
p.Ser124Phe
mcSCC444
mcSCC1310
mcSCC168
mcSCC131
c.628C>T
p.Arg210Cys
mcSCC124
c.823C>T
p.Pro275Ser
mcSCC272
mcSCC278
mcSCC876
c.824C>T
p.Pro275Leu
mcSCC874
c.289C>T
p.Gln97*
mcSCC446
c.50T>A
p.Leu17Gln
Trp53
69,400,442
69,401,057
69,401,870
69,401,878
60,401,892
69,402,025
69,402,160
69,402,149
69,403,100
69,403,109
69,403,124
69403125
B
mcSCC334
c.916T>C
p.Cys306Arg
mcSCC272
c.1366T>A
p.Cys456Ser
mcSCC873
c.637C>T
p.Pro213Ser
mcSCC272
c.1894G>T
p.Gly632*
mcSCC134
c.3409T>G
p.Tyr1137Asp
mcSCC164
c.7378C>T
p.Pro2460Ser
Notch1
26,339,893
26,336,677
26,335,466
26,333,599
26,326,443
26,315,269
C
mcSCC278
c.151T>G
p.Cys51Gly
mcSCC444
c.4061G>A
p.Gly1354Glu
mcSCC874
c.6140C>T
p.Pro2047Leu
Notch2
97,851,728
97,939,304
97,950,085
D
mcSCC168
c.5860G>A
p.Glu1954Lys
mcSCC876
c.368C>T
p.Pro123Leu
mcSCC164
c.676C>T
p.Leu226Phe
mcSCC134
c.4714C>T
p.Arg1572Cys
mcSCC876
c.6508C>T
p.Leu2170Phe
Notch3
32,295,678
32,295,370
32,278,187
32,261,283
32,259,214
E
mcSCC278
c.2653G>A
p.Ala885Thr
mcSCC876
c.4994C>T
p.Pro1665Leu
Notch4
34714498
34723111